Anomalous conduction in one-dimensional particle lattices: Wave-turbulence approach

Francesco De Vita,[1] Giovanni Dematteis [ID],[2,*] Raffaele Mazzilli [ID],[3] Davide Proment [ID],[4]
Yuri V. Lvov,[2] and Miguel Onorato [ID][5,6]

[1]*DMMM, Politecnico di Bari, Via Re David 200, Bari 70125, Italy*
[2]*Department of Mathematical Sciences, Rensselaer Polytechnic Institute, Troy, New York 12180, USA*
[3]*Max-Planck-Institut für Festkörperforschung, 70569 Stuttgart, Germany*
[4]*School of Mathematics, University of East Anglia, Norwich Research Park, NR4 7TJ Norwich, United Kingdom*
[5]*Dipartimento di Fisica, Università di Torino, Via P. Giuria 1, Torino 10125, Italy*
[6]*INFN, Sezione di Torino, Via P. Giuria 1, Torino 10125, Italy*

One-dimensional particle chains are fundamental models to explain anomalous thermal conduction in low-dimensional solids such as nanotubes and nanowires. In these systems the thermal energy is carried by phonons, i.e., propagating lattice oscillations that interact via nonlinear resonance. The average energy transfer between the phonons can be described by the wave kinetic equation, derived directly from the microscopic dynamics. Here we use the spatially nonhomogeneous wave kinetic equation of the prototypical β-Fermi-Pasta-Ulam-Tsingou model, to study thermal conduction in one-dimensional particle chains on a mesoscale description. By means of numerical simulations, we study two complementary aspects of thermal conduction: in the presence of thermostats setting different temperatures at the two ends and propagation of a temperature perturbation over an equilibrium background. Our main findings are as follows. (i) The anomalous scaling of the conductivity with the system size, in close agreement with the known results from the microscopic dynamics, is due to a nontrivial interplay between high and low wave numbers. (ii) The high-wave-number phonons relax to local thermodynamic equilibrium transporting energy diffusively, in the manner of Fourier. (iii) The low-wave-number phonons are nearly noninteracting and transfer energy ballistically. These results present perspectives for the applicability of the full nonhomogeneous wave kinetic equation to study thermal propagation.

I. INTRODUCTION

That heat conduction in three-dimensional macroscopic solids is described effectively by Fourier's law has been known for two centuries [1]. This law establishes the existence of a size-independent property of the material, the heat conductivity $\mathcal{K}$, as a finite proportionality constant between the heat flux and its driving thermodynamic force, the temperature gradient [2]. In low-dimensional solids this proportionality may break down and size-dependent conduction effects arise. One-dimensional (1D) particle chains characterized by harmonic potential have a conductivity proportional to the chain length L, that is, $\mathcal{K} \propto L^1$ [3]. The lattice excitations propagate unperturbed as noninteracting wave packets; this implies the absence of relaxation. Therefore, energy is transported by advection (or ballistically [4]), rather than by diffusion as prescribed by Fourier's law. Intermediate behaviors in which $\mathcal{K} \propto L^\alpha$, with $0 < \alpha < 1$, are observed both in numerical simulations of more realistic particle chains [5,6] and in experiments involving nearly 1D systems such as carbon nanotubes and silicon nanowires [7–12]. This type of transport, which is neither diffusive nor ballistic, is referred to as anomalous and its investigation, motivated by the relevance of the widespread technological applications, has generated a large body of literature in the past two decades [13].

A minimal model displaying anomalous transport is the Fermi-Pasta-Ulam-Tsingou (FPUT) chain [14,15], in which a cubic (α-FPUT) or quartic (β-FPUT) anharmonic term is added to the harmonic potential. Physically, this term represents the lowest-order nonlinear correction to the linearized harmonic system, in a power-law expansion of the potential around the equilibrium point. Weak nonlinearity plays a crucial role in the derivation of the so-called phonon Boltzmann equation, or wave kinetic equation (WKE) [16–20]. The WKE is the statistical closure of the deterministic equations of motion, for the spectral action density $n(k, t)$, i.e., the second moment of the random wavefield in Fourier space; $n(k, t)$ is related to the spectral energy density $e(k)$ via $e(k) = \omega(k)n(k)$, where $\omega(k)$ is the linear dispersion relation. The WKE contains the statistical description of the action or energy transfers between the various wave modes. These transfers are mediated by the collision integral, which incorporates the nonlinear terms in the WKE as wave-wave resonant interactions between the eigenstates of the harmonic chain, i.e., the linear waves. The timescales of the resonant transfers, the kinetic timescales, are much longer than the linear timescale of wave propagation, where the scale separation is tied to the smallness of the nonlinearity. For the β-FPUT chain. in the thermodynamic limit (large system), the quartic term in the potential yields a collision integral encoding four-wave resonant interactions [21–23] that exchange energy between quartets of wave modes and ultimately lead to relaxation over the kinetic timescales [24].

---

*Corresponding author: giovannidematteis@gmail.com

A kinetic interpretation of the numerically observed anomalous exponent $\alpha \simeq 0.4$ [25] in the β-FPUT system was proposed in [26] and given rigorous justification in [27,28]. The result is based on the relaxation-time approximation of the collision integral for the acoustic modes, as $k \to 0$, and on a subsequent heuristic cutoff applied to the linear-response Kubo integration of the correlation function [5]. In [29] an analogous asymptotic result was exploited to identify a critical scale k_c determining a separation between two sets of modes: Those with $|k| < k_c$ essentially behave as ballistic modes in a harmonic chain, as they lack a sufficient level of interaction, and the modes with $|k| > k_c$ are diffusive and relax locally to the expected Fourier profile. In this interpretation, the anomalous exponent is due to how the separation between the two sets scales with the chain length, given by a certain function $k_c(L)$. Rather than from an anomalous type of diffusion (such as fractionary diffusion), the anomalous transport properties thus arise from the coexistence of regular diffusion and advective effects that persist on macroscopic scales due to the properties of the collision integral.

Here we go beyond the asymptotic result for the acoustic modes and fully exploit the mesoscopic picture, by direct numerical integration in time of the spatially nonhomogeneous WKE associated with the β-FPUT model. We show that the first-principles description of the WKE is able to reproduce accurately the anomalous transport properties observed in the direct numerical simulations of the microscopic dynamics [13]. We also confirm results previously conjectured on the separation between ballistic modes and diffusive modes [29] and characterize the respective transport coefficients. Finally, we exploit the higher-level and computationally much cheaper picture of the WKE to investigate in detail the local relaxation properties of the different modes.

II. MODEL

To simulate thermal energy transfers through a one-dimensional particle chain, we solve the following space-dependent WKE, written in nondimensional form (see the Appendix for its nondimensionalization), associated with the β-FPUT model in the thermodynamic limit [24], for the spectral action density $n_k = n(x, k, t)$ [19,30–32]:

$$\frac{\partial n_k}{\partial t} + v_k \frac{\partial n_k}{\partial x} = \mathcal{I}_k. \tag{1}$$

We denote by $x \in [0, L]$, $k \in [0, 2\pi)$, and $t > 0$ the (macroscopic) physical space, the Fourier space, and the time variables, respectively. The second term on the left-hand side of (1) represents the advection of n_k due to spatial inhomogeneities, where $\omega_k = 2 \sin(k/2)$ is the linear dispersion relation and $v_k = d\omega_k/dk = \cos(k/2)$ is the group velocity; the right-hand side of (1) is the four-wave collision integral

$$\mathcal{I}_k = 4\pi\nu \int_0^{2\pi} |T_{k123}|^2 n_k n_{k_1} n_{k_2} n_{k_3} \left(\frac{1}{n_k} + \frac{1}{n_{k_1}} \right.$$
$$\left. - \frac{1}{n_{k_2}} - \frac{1}{n_{k_3}} \right) \delta(\Delta K) \delta(\Delta\Omega) dk_1 dk_2 dk_3, \tag{2}$$

where the arguments of the Dirac δ functions are defined as $\Delta K = k + k_1 - k_2 - k_3$ and $\Delta\Omega = \omega_k + \omega_1 - \omega_2 - \omega_3$,

$|T_{k123}|^2 = 9\omega_k \omega_1 \omega_2 \omega_3 / 16$ is the matrix element associated with the β-FPUT model [28,33], and ν is a nondimensional parameter that weights the collision integral defined as

$$\nu = \frac{\beta^2}{\chi^4} \frac{\lambda}{a} k_B^2 \bar{T}^2, \tag{3}$$

where $\bar{T}$ is the mean temperature of the chain, k_B is the Boltzmann constant, λ a typical macroscopic scale, a is the equilibrium interparticle distance, and χ and β are the coefficients of the quadratic (Hooke's law) and quartic terms of the interparticle potential in the microscopic description, respectively.

The integration of (2) has only one degree of freedom, since the resonance conditions imposed by the δ functions constrain the integration to the so-called resonant manifold, i.e., the subset of possible combinations of k_1, k_2, and k_3 that are in resonance with mode k, representing all the resonant wave quartets. We provide an explicit expression of this one-dimensional integration in the Appendix.

The resonant interactions contained in the collision integral represent the mechanism responsible for the local (i.e., at fixed x) relaxation to the equilibrium distribution of n_k which, given the two conserved quantities of (1), is given by the Rayleigh-Jeans (RJ) solution

$$n_k^{(\text{RJ})} = \frac{T}{\omega_k + \mu}. \tag{4}$$

Here T plays the role of a nondimensional temperature of the system and μ of the chemical potential; these quantities are associated with the conservation of the harmonic energy and of the action (or number of particles), respectively. The spatial energy density profile can be computed by multiplying n_k by ω_k and integrating in k:

$$e(x, t) = \int_0^{2\pi} \omega_k n(x, k, t) dk. \tag{5}$$

To avoid confusion, we recall that due to the discreteness of the physical space the Fourier space is periodic and therefore the modes in the interval $[\pi, 2\pi)$ can be equivalently interpreted as in $[-\pi, 0)$. For this reason, hereafter we refer to the modes near 0 or 2π as the low wave numbers and to the modes near π as the high wave numbers.

III. RESULTS

In what follows we discuss results achieved from two types of numerical simulations of the nonhomogeneous wave kinetic equation: Case A corresponds to the classical problem of a chain in between two thermostats at different temperatures and case B corresponds to the free evolution of an initial energy density narrow Gaussian profile in x. The latter is the typical experiment used to assess the diffusive (or nondiffusive) properties of the system.

A. Anomalous conduction

To demonstrate numerically anomalous conduction, we consider a domain of size L with two thermostats at its ends at different temperatures T_1 and T_2. For normal conduction, at the steady state one expects a linear temperature T profile (Fourier's law) and the conductivity $\mathcal{K}$ to be independent of
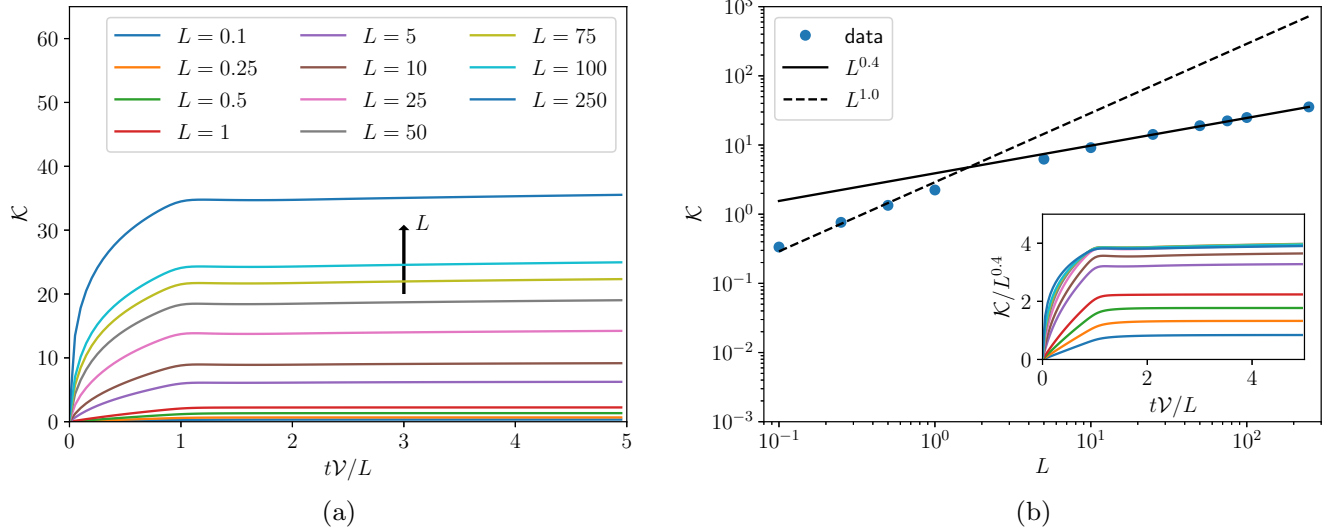
FIG. 1. (a) Thermal conductivity $\mathcal{K}$ as a function of nondimensional time for several values of L and (b) steady-state thermal conductivity $\mathcal{K}$ as a function of L. For small L most of the modes are noninteracting and the ballistic scaling $\mathcal{K} \propto L^1$ is recovered. For larger L we observe excellent asymptotic agreement with the scaling $\mathcal{K} \propto L^{0.4}$. The inset in (b) shows the thermal conductivity $\mathcal{K}$ in (a) normalized by $L^{0.4}$ as a function of nondimensional time.

the size of the domain L. By defining the net spectral energy current as

$$j(k,x,t) = \omega_k v_k [n(k,x,t) - n(-k,x,t)]/2, \quad (6)$$

the conductivity can be computed as

$$\mathcal{K} = \frac{JL}{\Delta T}, \quad (7)$$

with

$$J = \frac{1}{L} \int_0^L \int_0^{2\pi} j(k,x,t) dk\, dx \quad (8)$$

the spatial average of the integral of $j(k,x,t)$ and $\Delta T = T_1 - T_2$ the temperature difference between the two thermostats. The term $\Delta T/L$ represents the mean temperature gradient and one can recognize the definition of $\mathcal{K}$ as given by Fourier's law. Note that, at the steady state, the energy current is independent of x.

In Fig. 1(a) we show the time history of the conductivity for several values of the domain size L, keeping ΔT fixed. The initial ($t = 0$) distribution is set to be a RJ distribution at the average temperature between the two thermostats; subsequently, there is an initial transient during which the energy flux starts growing (and consequently also $\mathcal{K}$), until a stationary state is reached. Note that time is scaled with the reference time $L/\mathcal{V}$, with $\mathcal{V} = v_{k=0} = 1$ the maximal ballistic velocity. In Fig. 1(b) we show the measured conductivity as a function of the domain size L. The results clearly indicate that for small L the stationary value of the conductivity tends to be proportional to L, as in the purely harmonic system. In contrast, for $L \to \infty$ the exponent α tends to the constant value of 0.4, consistent with the value measured in the microscopic simulations [25]. In the inset of the figure, the time history of the conductivity $\mathcal{K}$ divided by $L^{0.4}$ is drawn to highlight that for large values of L the curves overlap.

Via integration of the deterministic microscopic equations, a recent work [29] provided evidence that the collision integral

$\mathcal{I}_k$ brings the system to local equilibrium down to a critical k_c, whereas for lower k advection is predominant and waves travel in the domain transported by the group velocity v_k interacting too weakly to relax locally to a RJ spectrum. Here we observe this clearly by looking at the evolution of the colormap of the temperature in Fig. 2, where the temperature spectral density $T(x,k,t) = (\omega_k + \mu)n(x,k,t)$ is defined by inverting (4), using the fact that μ is constant throughout the evolution. Note that for $k < \pi$ the velocity v_k is positive, while it is negative for $k > \pi$. The initial condition at $t = 0$ is a homogeneous field, with $n(x,k,t=0) = n_k^{(\mathrm{RJ})}$ at temperature $(T_1 + T_2)/2$. Due to the presence of the thermostats, as $t > 0$ the waves going to the right start to propagate a hot front from the left thermostat, while the waves going to the left start propagating a cold front from the right thermostat. The edge of the front propagates at the maximal speed allowed, which is the speed of the acoustic modes $v(k \to 0^\pm) = \pm 1$. For $L = 1$, the energy flows in a ballistic way for almost the entire domain and the collision integral is not strong enough to bring the system to local equilibrium. As a result, at large times and at any fixed point x, the right-going waves are at temperature T_1 and the left-going waves are at temperature T_2, far from local equipartition. For larger system size $L = 10$ instead, advection is predominant only in a small range of k, with the remaining part of the domain dominated by diffusion: In this region, at large time and at any fixed point x, the energetic content of the left- and right-going waves is equipartitioned and there is a constant smooth temperature gradient between the two thermostats. This is reflected in the profile in k of the spatial integral of the spectral energy current $\langle j \rangle_x = \frac{1}{L} \int_x j(k,x)dx$, once a steady state is reached [see Fig. 3(a)]. For modes with small k, $\langle j \rangle_x$ is independent of the system size since the behavior is purely ballistic [3]. For modes with large k the energy current flattens as L increases, accompanied by a reduction of the peak value. In particular, Fig. 3(b) shows how for these modes the energy current is inversely proportional to
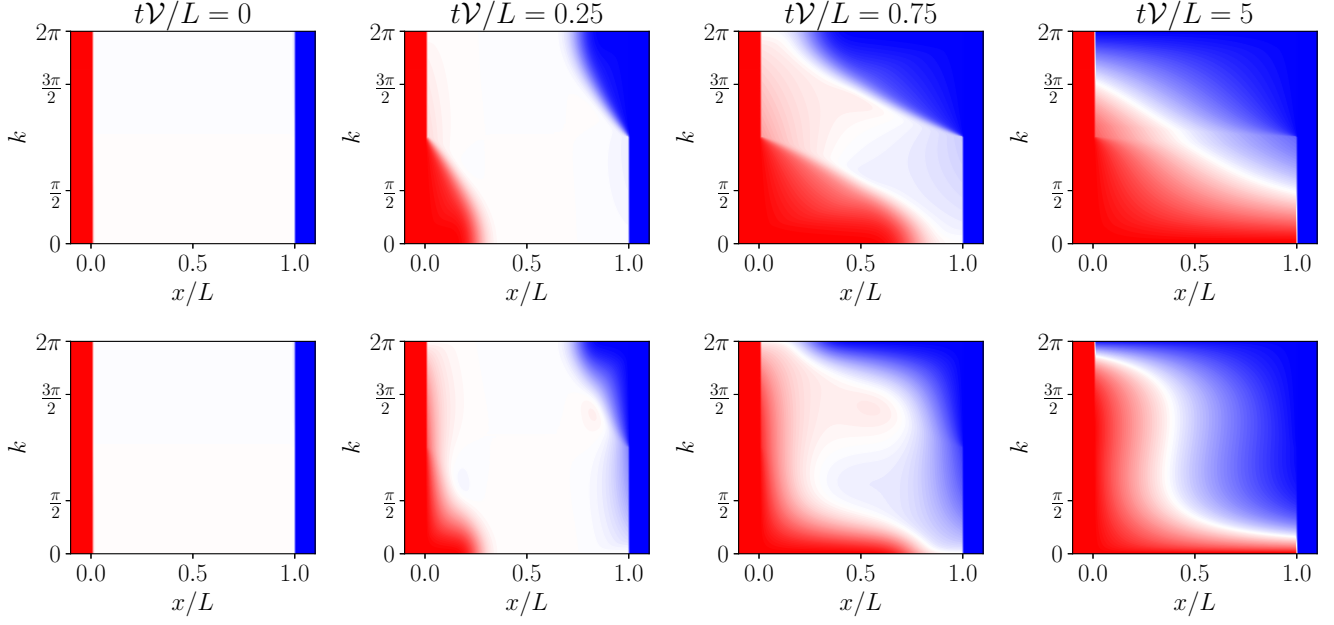
FIG. 2. Colormap of $T(x, k, t) = (\omega_k + \mu)n(x, k, t)$ for $L = 1$ (top row) and $L = 10$ (bottom row). Color ranges from T_2 (white) to T_1 (red). For $t > 0$, two fronts start propagating the temperature of the thermostats, perturbing the initial homogeneous state. The modes in $[0, \pi]$ propagate to the right ($v_k > 0$) and the modes in $[\pi, 2\pi]$ propagate to the left ($v_k < 0$). The top panels depict a predominantly ballistic situation also at the stationary state (rightmost panel), since L is not sufficiently large for most of the modes to interact. For the larger system in the bottom panels, once a steady state is reached the diffusive modes (around $k = \pi$) have equipartitioned at fixed x and are accompanied by a k-independent constant gradient between the two thermostats. On the other hand, the ballistic modes (around $k = 0$ and $k = 2\pi$) carry the energy density of their originating thermostat all the way to the opposite side without interactions with other modes. Here we observe that the width of the ballistic region becomes thinner as L increases (see Fig. 4).

the chain length L, as one would expect from Fourier's law, i.e., (7) when $\mathcal{K}$ does not depend on L. There should then be a critical value k_c above which the evolution of the energy is diffusion dominated and below which the predominant transport mechanism is the purely ballistic one. Considering

that at equilibrium the transport term and the collision integral should balance and using dimensional arguments, one can find that $k_c \approx L^{-3/10}$ [29]. Note that this estimation relies on an asymptotic approximation of the collision integral for small k, since the lack of scale invariance in the operator (2) does
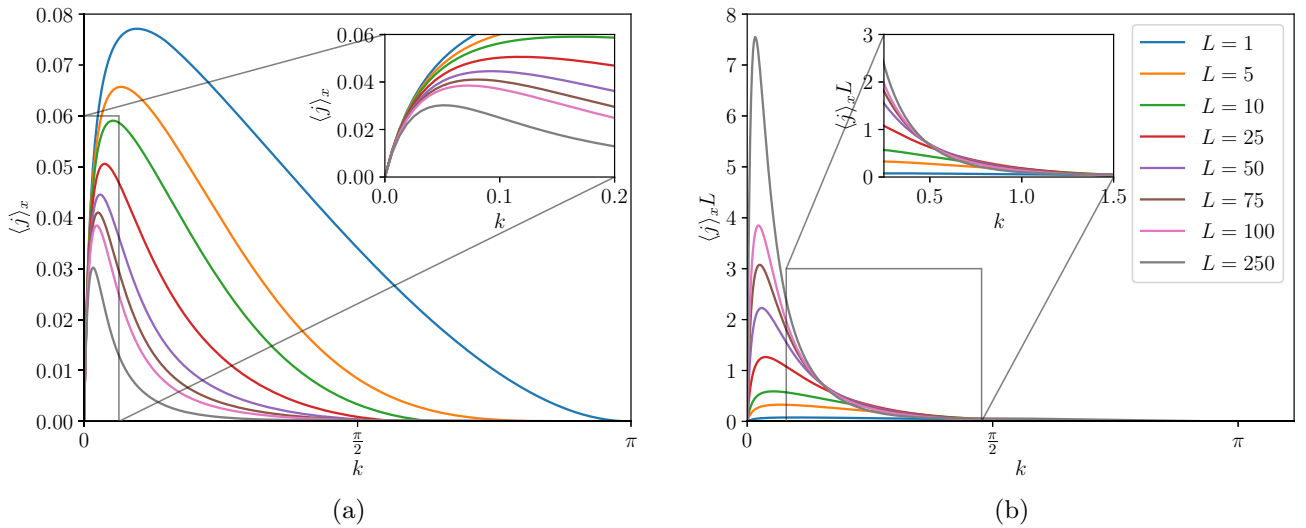

FIG. 3. (a) Energy current $\langle j \rangle_x$ as a function of k for different domain sizes, once a steady state has been reached. While for the high wave numbers the energy current contribution decreases as L increases, the low-wave-number contribution is independent of L, in agreement with ballistic behavior. In the inset, one can appreciate this invariance as $k \to 0$. (b) Energy current $\langle j \rangle_x$ multiplied by the size of the domain L. Now the renormalized curves tend to converge onto each other independently of L for the high wave numbers. This behavior is in agreement with Fourier's law [see (7)] prescribing inverse proportionality between energy current and system size.
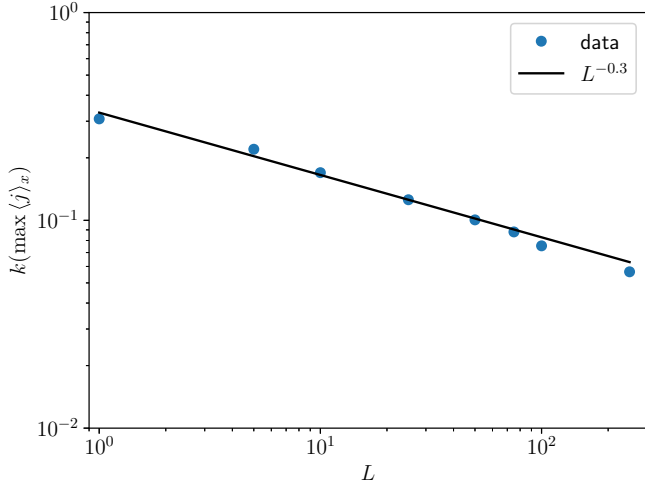
FIG. 4. Scaling of $k(\max\langle j\rangle_x)$ [defined as the point of maximum in Fig. 3(a)] as a function of L. The observed scaling is consistent with $L^{-0.3}$, which implies an anomalous exponent $\alpha = 0.4$.

not allow one to find simpler solutions as in [34]. A scaling consistent with the estimation in [29] can be found, in our simulations, for the value of k for which $\langle j\rangle_x$ is maximal, as shown in Fig. 4, suggesting that this criterion could be used as a proxy for the determination of $k_c(L)$ to distinguish between diffusive and ballistic modes.

B. Ballistic and diffusive propagation

In nonequilibrium statistical physics, the transport coefficients characterizing nonequilibrium steady states that are not too far from equilibrium can be computed in terms of space-time correlations in an equilibrium ensemble of realizations of the microscopic dynamics [2,5,27,35,36], via the so-called Kubo integral. Likewise, for the mesoscopic

model of (1), let us now consider an initial background equilibrium state with constant $T = T_0$ and chemical potential μ. Let us then consider an initial narrow bell-shaped perturbation $\delta T(x)$ in the center of the domain such that $\delta T \ll T_0$. We initialize $n(x, k, t = 0)$ with a RJ distribution [see (4)] with $T(x) = T_0 + \delta T(x)$, in a domain going from $-L$ to L.

The evolution of $\langle n\rangle_k(x, t) = \int_0^{2\pi} n(x, k, t)dk$ is shown in Fig. 5, where we consider a perturbation having an initial amplitude of $\delta T(x = 0)/T_0 = 0.1$. One can recognize the familiar behavior of a central peak (heat peak) and two traveling peaks (acoustic peaks) which correspond to the emission of the second sound. This configuration has been studied using microscopic dynamics [5,35] and the stochastic model known as fluctuating hydrodynamics [36]. For $t > 0$, two peaks separate and propagate in opposite directions with constant velocity about ± 1; the central peak instead evolves diffusively in time [Fig. 5(a)]. This is clearly visible by looking at the time evolution of the variance of the distribution, computed as follows:

$$\sigma^2 = \frac{\int_{x,k} n(k, x, t)\omega(k)x^2 dx\, dk}{\int_{x,k} n(k, x, t)\omega(k)dx\, dk}. \tag{9}$$

Indeed, as shown in Fig. 5(b), after the acoustic peaks exit the domain (at about $t\mathcal{V}/L = 1$) and the central peak is left alone, the variance starts to grow linearly in time. The time evolution of the central peak follows regular diffusion, with the diffusion coefficient given by half the slope of the asymptote on the right-hand side of Fig. 5(b). This particular result may seem controversial in the face of notable results advocating for a heat peak that follows fractional diffusion (of superdiffusive type). We address this further in Sec. IV.

We can therefore identify the second sound emission with the nondecaying transport of the ballistic modes and the heat peak with the regular diffusion of the modes that thermalize locally. Further confirmation of this is found in Fig. 6,
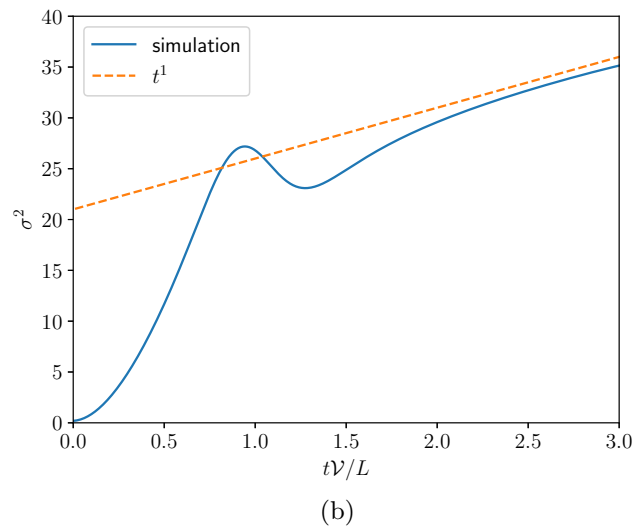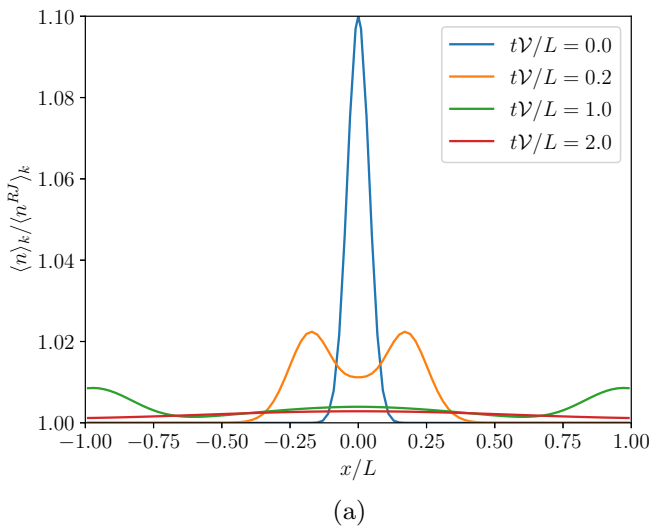

(a)

(b)

FIG. 5. (a) Spatial distribution of $\langle n\rangle_k(x, t)$ (integrated in k) at different times. An initial spatially localized perturbation over a uniform background propagates as two ballistic peaks moving in opposite directions at constant velocity and a central decaying peak. (b) Time history of the variance of the temperature distribution. After the ballistic peaks exit the system, the broadening of the central peak (also known as the heat peak) shows agreement with diffusive behavior.
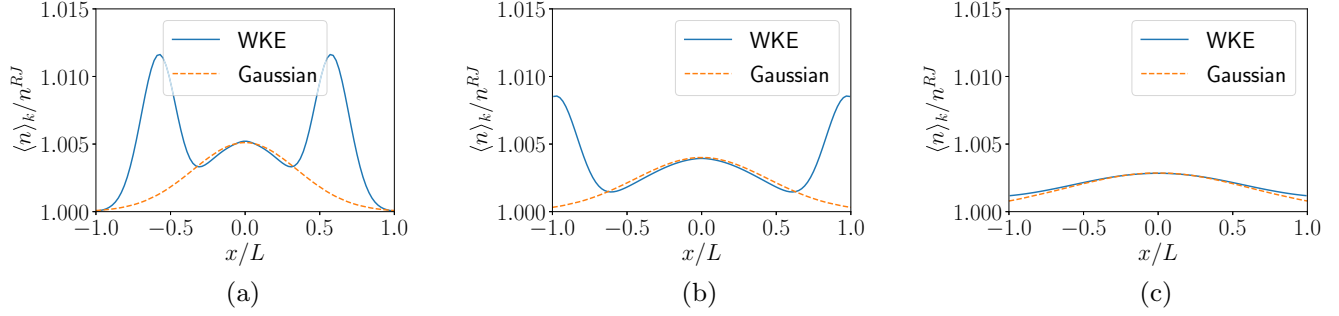
FIG. 6. Heat peak evolution as predicted by WKE (–) and pure diffusion (- -) for (a) $t\mathcal{V}/L = 0.6$, (b) $t\mathcal{V}/L = 1.0$, and (c) $t\mathcal{V}/L = 2.0$.

where we plot the time evolution of the small initial Gaussian perturbation on a homogeneous background and we show that the numerical simulation of the WKE follows closely a diffusive solution with diffusion coefficients around 0.24 for this condition. Thus, we can simply refer to the heat and the acoustic peaks as the diffusive and the ballistic (or second sound) peaks, respectively, without ambiguity. Figure 7 shows the energy density $e(x, k, t)$ at various times of the evolution of the perturbation. The low modes, with $k \approx 0$ and $k \approx 2\pi$, are the ones with the highest ballistic velocity. Hence, they will leave the domain in a timescale of the order of $L/\mathcal{V}$. For longer times, the higher modes start to diffuse due to the collision integral and the distribution will start to follow a diffusive evolution.

IV. DISCUSSION

Our direct numerical simulation of the WKE shows that two phononic states coexist in the β-FPUT chain. The first, involving the low modes, is equivalent to the emission of second sound; the second, involving the higher modes, is purely diffusive. This has been analyzed from the following different points of view.

(i) The anomalous scaling of the energy conductivity $\mathcal{K} \propto L^\alpha$, with $\alpha \simeq 0.4$, was confirmed in Fig. 1. This is due to the scaling $k_c(L)$ of the separation between the ballistic modes (low wave numbers) and the diffusive modes (high wave

numbers), individually contributing towards $\alpha = 1$ and $\alpha = 0$, respectively. We found that k_c varies consistently with L by the scaling $k_c(L) \propto L^{-3/10}$, as shown in Fig. 4.

(ii) The spatial integral of the spectral energy current modal density $\langle j \rangle_x(k)$ is independent of L for the low modes, as predicted for the purely harmonic chain [3], while it is proportional to L^{-1} for the higher modes, in agreement with Fourier's law. This was shown in Fig. 3.

(iii) A complementary way to analyze energy transport is to look at the evolution of a small localized perturbation of the thermal equilibrium condition. By doing that, we confirmed the presence of two acoustic peaks shooting off in opposite directions and a central heat peak [Fig. 5(a)] evolving in agreement with standard Fourier diffusion, as confirmed in Figs. 5(b) and 6(a)–6(c).

(iv) The existence of two types of heat transfer, ballistic and diffusive, was cleanly demonstrated in Figs. 2 and 7. In Fig. 2 the qualitative difference between these two types is most evident near the stationary nonequilibrium state, where the horizontal separation between the two different regions gives an intuitive visualization of k_c. Finally, in Fig. 7 we saw an *x-k* representation of the evolution of a perturbed equilibrium state. Again, the sharp separation wave number k_c could be observed by eye. Not surprisingly, we discovered that the acoustic peaks are made exclusively of noninteracting ballistic modes with low wave number, while the heat peak is made exclusively of modes with high wave number.
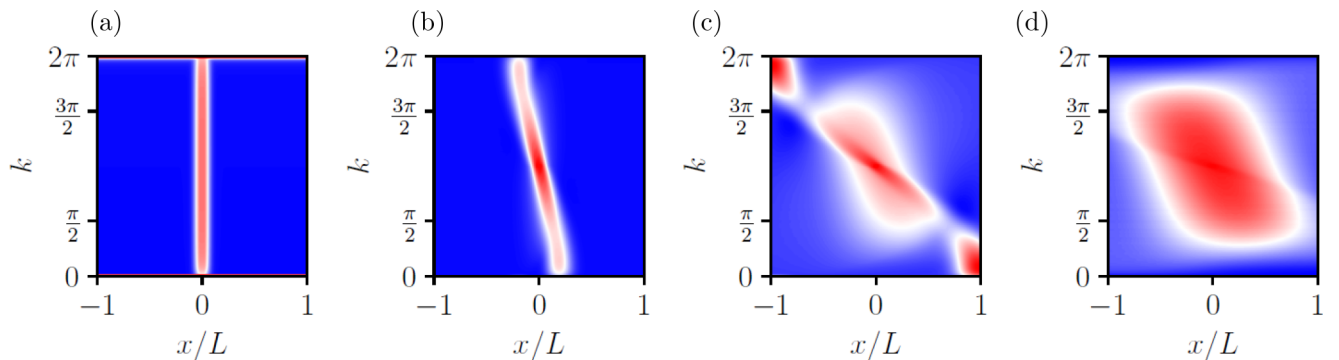

FIG. 7. Colormap of $e(x, k, t) = \omega_k n(x, k, t)$ at four nondimensional time instants: (a) $t\mathcal{V}/L = 0$, (b) $t\mathcal{V}/L = 0.2$, (c) $t\mathcal{V}/L = 1.0$, and (d) $t\mathcal{V}/L = 2.0$. The second sound emission is clearly seen in the central maps where perturbations at $k \simeq 0$ and $k \simeq 2\pi$ (the low modes) are detaching from the central diffusive peak involving the high modes. The interacting and diffusive character of these modes is evident from the fact that the shape of the central peak remains close to a rectangle during the evolution, tending to populate all modes k with the same energy density at fixed position x.

Although the separation of scales at k_c observed in the x-k plots was slightly smeared, the two-state ballistic-diffusive picture analyzed above under these four different angles is robust and does not include superdiffusive propagation with fractionary exponents. A fractionary diffusion equation with space derivative of order $\frac{8}{5}$ instead of 2 is an alternative explanation compatible with the conductivity scaling $K \propto L^{2/5}$, rigorously derived in [37]. However, this scaling would predict the propagation of a single peak that does not find correspondence in our observations. The apparent disagreement may have different origins. For example, the assumption of having only two conserved quantities (energy and action) made in [37] is partially violated by the ballistic modes, which effectively preserve momentum and whose propagation is not a part of the heat peak. Although we have assessed overall compatibility of the heat peak evolution with diffusive behavior, providing a definitive study of this issue is not the aim of the present paper. In close analogy with second sound propagation in superfluids [38], our results show that if the ballistic phonons are recognized as noninteracting traveling waves [29,39,40], the two-state ballistic-diffusive picture is compatible with the main observable aspects of energy transport.

One important aspect to stress is the computational and practical convenience of the wave kinetic equation. When studying the system on a microscopic level (i.e., solving the bare equations of motion of β-FPUT chains) it is necessary to perform simulations for a large number of different initial conditions to get converged ensemble statistics. In contrast, the simulation of the wave kinetic equation allows one to directly obtain results for the deterministic average spectral density, on a mesoscopic scale.

Finally, it is worth noting that second sound in dielectric solids was predicted a long time ago [41–43] and later observed, for instance, in solid ^{3}He and ^{4}He below 4 K and in NaF below 20 K, at extremely low temperature. In a dielectric crystal, second sound can be observed when umklapp resonances are very small, and by lowering the temperature enough, the scattering level is reduced to a point where noninteracting wavelike transport becomes visible on macroscopic scales. It is now well known that reducing the dimensionality of the material is another way to reduce drastically the number of interactions, in part explaining why it was recently possible to observe second sound propagation in 2D graphite at temperatures above 100 K [44,45]. Our results further indicate that reducing the dimensionality to (quasi-)1D structures such as nanotubes may allow for the possibility to finally observe second sound propagation at room temperature.

APPENDIX

1. Physical dimensions

We refer to the Hamiltonian equations for the β-FPUT chain derived in [33]. The Hamiltonian of the microscopic system in dimensional form is given by

$$\mathcal{H} = \sum_{j=1}^{N-1} \left(\frac{1}{2m}p_j^2 + \frac{\chi}{2}(q_j - q_{j-1})^2 + \frac{\beta}{4}(q_j - q_{j-1})^4 \right),$$
(A1)

where the q_j and p_j variables are the positions (more precisely, the displacements from the equilibrium positions) and momenta. The angular frequency and phase velocity are given in dimensional form by

$$\tilde{\omega}_k = 2\sqrt{\frac{\chi}{m}}\sin\left(\frac{a\tilde{k}}{2}\right), \quad \tilde{v}_k = \frac{d\tilde{\omega}}{d\tilde{k}} = a\sqrt{\frac{\chi}{m}}\cos\left(\frac{a\tilde{k}}{2}\right),$$
(A2)

respectively, where we use tildes to indicate dimensional variables. The WKE associated with the Hamiltonian in Eq. (A1) is

$$\frac{\partial \tilde{n}_k}{\partial \tilde{t}} + \tilde{v}_k \frac{\partial \tilde{n}_k}{\partial \tilde{x}} = \tilde{\mathcal{I}}_k,$$
(A3)

where

$$\tilde{\mathcal{I}}_k = 4\pi \frac{\beta^2}{\chi^4} \int_0^{2\pi} |\tilde{T}_{k123}|^2 \tilde{n}_k \tilde{n}_{k_1} \tilde{n}_{k_2} \tilde{n}_{k_3} \left(\frac{1}{\tilde{n}_k} + \frac{1}{\tilde{n}_{k_1}} \right.$$
$$\left. - \frac{1}{\tilde{n}_{k_2}} - \frac{1}{\tilde{n}_{k_3}} \right) \delta(\Delta\tilde{K})\delta(\Delta\tilde{\Omega}) d\tilde{k}_1 d\tilde{k}_2 d\tilde{k}_3,$$
(A4)

with

$$|\tilde{T}_{k123}|^2 = \tfrac{9}{16}\tilde{\omega}_k \tilde{\omega}_1 \tilde{\omega}_2 \tilde{\omega}_3.$$
(A5)

Let us introduce the following dimensionless variables (denoted without a tilde):

$$x = \frac{1}{\lambda}\tilde{x}, \quad v_k = \frac{1}{a}\sqrt{\frac{m}{\chi}}\tilde{v}_k, \quad t = \frac{a}{\lambda}\sqrt{\frac{\chi}{m}}\tilde{t},$$

$$n_k = \frac{1}{k_B\tilde{T}a}\sqrt{\frac{\chi}{m}}\tilde{n}_k, \quad \omega_k = \sqrt{\frac{m}{\chi}}\tilde{\omega}_k, \quad k = a\tilde{k}.$$
(A6)

Plugging these nondimensional variables in Eqs. (A3)–(A5), we obtain Eqs. (1)–(3), now in a nondimensional form.

2. Integration on the resonant manifold

In (2), the equality coming from the momentum Dirac δ has to be interpreted as mod$I$, $I = [0, 2\pi)$, to include possible umklapp resonances. The resonant manifold is the subset of $I \times I \times I \times I$ satisfying at the same time the two conditions

$$\omega_k + \omega_{k_1} - \omega_{k_2} - \omega_{k_3} = 0, \quad k_3 = (k + k_1 - k_2)\text{mod}I.$$
(A7)

The constraint imposed by integration on the resonant manifold reduces the triple integral of (2) to a one-dimensional

integral. Here we briefly report some important rigorous results from Ref. [28] (see also [26,35]). The solutions of the collisional constraints (A7) are of three types (i) $k_1 = k_3$ and $k_2 = k_4$, (ii) $k_1 = k_4$ and $k_2 = k_3$, and (iii) $k_2 = h(k_1, k_3) \bmod I$, where

$$h(x, y) = \frac{y - x}{2} + 2 \arcsin\left(\tan \frac{|y - x|}{4} \cos \frac{y + x}{4}\right). \quad \text{(A8)}$$

The first two types (perturbative solutions) are trivial resonances that contribute to nonlinear frequency shift and broadening [24]. The third type of solutions (nonperturbative) represents nontrivial resonances that are responsible for irreversible spectral transfers. By integrating analytically in k_3, the collision integral of (2) can be written as

$$\mathcal{I}_k = \int_0^{2\pi} dk_1 dk_2 g(k, k_1, k_2) \delta(\Omega(k, k_1, k_2)), \quad \text{(A9)}$$

with

$$
\begin{aligned}
g(k, k_1, k_2) = {} & 4\pi |T_{k,k_1,k_2,k+k_1-k_2}|^2 n_k n_{k_1} n_{k_2} n_{k+k_1-k_2} \\
& \times \left(\frac{1}{n_k} + \frac{1}{n_{k_1}} - \frac{1}{n_{k_2}} - \frac{1}{n_{k+k_1-k_2}}\right),
\end{aligned}
$$

$$\Omega(k, k_1, k_2) = \omega_k + \omega_{k_1} - \omega_{k_2} - \omega_{k+k_1-k_2}. \quad \text{(A10)}$$

In order to integrate out the frequency δ, we exploit the following property of the Dirac δ function:

$$\int dx\, G(x) \delta(f(x)) = \int dx\, G(x) \sum_i \frac{\delta(x - x_i^\star)}{|f'(x_i^\star)|}. \quad \text{(A11)}$$

Here $x_i^\star$ are all the zeros of f. In (A9), integrating in the variable k_1, we know that all of the zeros of $\Omega = 2[\sin(k/2) + \sin(k_1/2) - \sin(k_2/2) - \sin(|k + k_1 - k_2|/2)]$ are of one of the three types above. The trivial solutions give $\Omega'(k_1) = 0$ identically, which implies singular denominators. However,, as discussed in Ref. [28], these terms come in pairs of opposite sign [this can be seen easily looking at the symmetries of the integrand of (2)], which cancel each other and do not contribute. Therefore, the nonvanishing contributions come from the nontrivial resonances and we obtain

$$
\begin{aligned}
\mathcal{I}_k &= \int_0^{2\pi} dk_2 \int_0^{2\pi} dk_1 g(k, k_1, k_2) \frac{\delta(k_1 - h(k, k_2))}{|\partial_{k_1} \Omega(k, h(k, k_2), k_2)|} \\
&= \int_0^{2\pi} dk_2 \frac{g(k, h(k, k_2), k_2)}{\sqrt{\left(\cos \frac{k}{2} + \cos \frac{k_2}{2}\right)^2 + 4 \sin \frac{k}{2} \sin \frac{k_2}{2}}}. \quad \text{(A12)}
\end{aligned}
$$

3. Numerical details

Equation (1) is solved by finite-difference approximation in time and space, using the expression of $\mathcal{I}_k$ given in (A12). In all simulations, we used 100 grid points in x and 1001 points in k; the chemical potential is set to $\mu = 0.05$. Without loss of generality, for the purpose of our work we have set $\nu = 1$. The adopted discretization guarantees the conservation of energy and wave action. In case A of Sec. III we used $T_1 = 0.4$ and $T_2 = 0.2$. In case B of Sec. III we used $T_0 = 0.3$ and $\delta T (x = 0)/T_0 = 0.1$.

[1] J. B. J. Fourier, *Théorie Analytique de la Chaleur* (Didot, Paris, 1822).

[2] R. Kubo, M. Toda, and N. Hashitsume, *Statistical Physics II: Nonequilibrium Statistical Mechanics*, edited by P. Fulde, Springer Series in Solid-State Sciences Vol. 31 (Springer, Berlin, 2012).

[3] Z. Rieder, J. Lebowitz, and E. Lieb, J. Math. Phys. **8**, 1073 (1967).

[4] A. Dhar and K. Saito, in *Thermal Transport in Low Dimensions: From Statistical Physics to Nanoscale Heat Transfer*, edited by S. Lepri, Lecture Notes in Physics Vol. 921 (Springer, Berlin, 2016), pp. 39–105.

[5] S. Lepri, R. Livi, and A. Politi, Phys. Rep. **377**, 1 (2003).

[6] D. Donadio and G. Galli, Phys. Rev. Lett. **102**, 195901 (2009).

[7] C. W. Chang, D. Okawa, H. Garcia, A. Majumdar, and A. Zettl, Phys. Rev. Lett. **101**, 075903 (2008).

[8] J. Chen, G. Zhang, and B. Li, Nano Lett. **10**, 3978 (2010).

[9] S. Shen, A. Henry, J. Tong, R. Zheng, and G. Chen, Nat. Nanotechnol. **5**, 251 (2010).

[10] N. Yang, G. Zhang, and B. Li, Nano Today **5**, 85 (2010).

[11] S. Liu, X. Xu, R. Xie, G. Zhang, and B. Li, Eur. Phys. J. B **85**, 337 (2012).

[12] C.-W. Chang, in Thermal Transport in Low Dimensions: From Statistical Physics to Nanoscale Heat Transfer (Ref. [4]), pp. 305–338.

[13] Thermal Transport in Low Dimensions: From Statistical Physics to Nanoscale Heat Transfer (Ref. [4]).

[14] E. Fermi, J. Pasta, and S. Ulam, Studies of nonlinear problems, I, Los Alamos Scientific Laboratory Report No. LA-1940 (Los Alamos Scientific Laboratory, Los Alamos, NM, 1955).

[15] *The Fermi-Pasta-Ulam Problem*, edited by G. Gallavotti, Lecture Notes in Physics Vol. 728 (Springer, Berlin, 2007).

[16] R. Peierls, Ann. Phys. (NY) **395**, 1055 (1929).

[17] V. E. Zakharov, V. S. L'vov, and G. Falkovich, *Kolmogorov Spectra of Turbulence I: Wave Turbulence* (Springer, Berlin, 2012).

[18] Y. Choi, Y. V. Lvov, and S. Nazarenko, Physica D **201**, 121 (2005).

[19] S. Nazarenko, *Wave Turbulence*, Lecture Notes in Physics Vol. 825 (Springer, Berlin, 2011).

[20] G. L. Eyink and Y.-K. Shi, Physica D **241**, 1487 (2012).

[21] S. Chibbaro, G. Dematteis, C. Josserand, and L. Rondoni, Phys. Rev. E **96**, 021101(R) (2017).

[22] S. Chibbaro, G. Dematteis, and L. Rondoni, Physica D **362**, 24 (2018).

[23] M. Onorato and G. Dematteis, J. Phys. Commun. **4**, 095016 (2020).

[24] Y. V. Lvov and M. Onorato, Phys. Rev. Lett. **120**, 144301 (2018).

[25] S. Lepri, R. Livi, and A. Politi, Europhys. Lett. **43**, 271 (1998).

[26] A. Pereverzev, Phys. Rev. E **68**, 056124 (2003).

[27] K. Aoki, J. Lukkarinen, and H. Spohn, J. Stat. Phys. **124**, 1105 (2006).

[28] J. Lukkarinen and H. Spohn, Commun. Pure Appl. Math. **61**, 1753 (2008).

[29] G. Dematteis, L. Rondoni, D. Proment, F. De Vita, and M. Onorato, Phys. Rev. Lett. **125**, 024101 (2020).

[30] Y. Deng and Z. Hani, arXiv:2104.11204.

[31] I. Ampatzoglou, C. Collot, and P. Germain, arXiv:2107.11819.

[32] M. Rosenzweig and G. Staffilani, Physica D **433**, 133148 (2022).

[33] M. D. Bustamante, K. Hutchinson, Y. V. Lvov, and M. Onorato, Commun. Nonlinear Sci. Numer. Simulat. **73**, 437 (2019).

[34] S. Nazarenko, A. Soffer, and M.-B. Tran, Entropy **21**, 823 (2019).

[35] J. Lukkarinen, in Thermal Transport in Low Dimensions: From Statistical Physics to Nanoscale Heat Transfer (Ref. [4]), pp. 159–214.

[36] H. Spohn, in Thermal Transport in Low Dimensions: From Statistical Physics to Nanoscale Heat Transfer (Ref. [4]), pp. 107–158.

[37] A. Mellet and S. Merino-Aceituno, J. Stat. Phys. **160**, 583 (2015).

[38] V. P. Peshkov *et al.*, Helium **4**, 166 (2013).

[39] V. A. Kuzkin and A. M. Krivtsov, Phys. Rev. E **101**, 042209 (2020).

[40] V. A. Kuzkin and A. M. Krivtsov, Acta Mech. **232**, 1983 (2021).

[41] M. Chester, Phys. Rev. **131**, 2013 (1963).

[42] E. Prohofsky and J. Krumhansl, Phys. Rev. **133**, A1403 (1964).

[43] D. Chandrasekharaiah, ASME Appl. Mech. Rev. **39**, 355 (1986).

[44] S. Huberman, R. A. Duncan, K. Chen, B. Song, V. Chiloyan, Z. Ding, A. A. Maznev, G. Chen, and K. A. Nelson, Science **364**, 375 (2019).

[45] G. Chen, Nat. Rev. Phys. **3**, 555 (2021).